Available online at www.sciencedirect.com
SCIENCE DIRECT®
Remote Sensing of Environment 100 (2006) 114 – 132
Remote Sensing of Environment
www.elsevier.com/locate/rse

3D modelling of forest canopy structure for remote sensing simulations in the optical and microwave domains

M. Disney *, P. Lewis, P. Saich

Department of Geography, University College London, 26 Bedford Way, London WC1H 0AP, United Kingdom
NERC Centre for Terrestrial Carbon Dynamics, United Kingdom

Received 7 July 2005; received in revised form 4 October 2005; accepted 8 October 2005

Abstract

A detailed 3D structural model of a conifer forest canopy was developed in order to simulate the reflectance (optical) and backscatter (microwave) signals measured remotely. We show it is feasible to model forest canopy scattering using detailed 3D models of tree structure including the location and orientation of individual needles. An existing structural growth model of Scots pine (*Pinus sylvestris* L.), Treegrow, was modified to simulate observed growth stages of a Scots pine canopy from age 5 to 50 years. The 3D tree models showed close structural agreement with in situ measurements. Needles were added to the structural models according to observed phyllotaxy (distribution). Individual trees were used to generate model canopies, which in turn were used to drive optical and microwave models of canopy scattering. Simulated canopy radiometric response was compared with airborne hyperspectral reflectance data (HyMAP) and airborne synthetic aperture RADAR (ASAR) backscatter data. Model simulations agreed well in general with observations, particularly at optical wavelengths where model simulations of low and high density canopy stands were shown to bracket observations. Relatively small sensitivity of observed reflectance to canopy age was captured reasonably well by the simulations. The choice of needle shape and phyllotaxy was shown to have a significant impact on multiple scattering behaviour at the branch scale. In the microwave domain, simulated backscatter values agreed reasonably well with observations at L-band, less so at X-band. L-band simulated backscatter significantly underestimated observed backscatter at younger canopy ages, probably as a result of inappropriate modelling of soil/understory. It is demonstrated that a combined structural and radiometric modelling approach provides a flexible and powerful method for simulating the remotely sensed signal of a forest canopy in the optical and microwave domains. This is particularly useful for exploring the impact of canopy structure on the resulting signal and also for combined retrievals of forest structural parameters from optical and microwave data.

Keywords: 3D canopy structure; Optical; Microwave; Scots pine; Biophysical parameters; Inversion; Look-up-table

1. Introduction

Vegetation canopy structure is known to have a significant impact on the Earth Observation (EO) signal in both the optical (Knyazikhin et al., 1998a,b; Panferov et al., 2001; Ross, 1981; Widlowski et al., 2004) and microwave (Imhoff, 1995) domains. This fact has been exploited through the development of forward models of canopy scattering (Goel, 1988; Goel & Thompson, 2000; Pinty & Verstraete, 1991). A large number of different approaches to such modelling have been taken, with different assumptions and simplifications made for different applications. As an example, scattering in the optical domain from relatively homogeneous canopy types (cereals, grasses) typically requires some form of radiative transfer (RT) approach to describe the (dominant) volume scattering behaviour of the canopy–soil system (Myneni et al., 1989; Qin & Liang, 2000; Ross, 1981). In contrast, the optical scattering behaviour of more heterogeneous canopies (in terms of 3D arrangement of scattering objects), such as forest canopies consisting of numerous tree crowns with relatively large gaps between them, tends to be dominated by the macroscopic properties of illuminated and shadowed crown and ground components. This can be modeled through the use of geometric–optics (GO) (Li & Strahler, 1985, 1986). Many intermediate modelling approaches have also been developed

* Corresponding author. Department of Geography, University College London, 26 Bedford Way, London WC1H 0AP, United Kingdom. Tel.: +44 207 679 4290.
E-mail address: mdisney@geog.ucl.ac.uk (M. Disney).

0034-4257/$ - see front matter © 2005 Elsevier Inc. All rights reserved.
doi:10.1016/j.rse.2005.10.003

to describe canopies characterized by some mixture of both volumetric and GO scattering in the optical domain (Goel, 1992, 1989; Strahler, 1996).

Different scattering processes dominate canopy scattering behaviour at optical and microwave wavelengths. In the optical (and shortwave IR) domain (i.e. wavelength λ ~0.4 to 0.7 μm for visible, up to ~1.4 μm in the NIR), scattering as a function of wavelength is predominantly controlled by the spectral reflectance, absorptance and transmittance properties of all material within the canopy, in particular green leaf material. Angular variation of the scattered radiation field is predominantly controlled by the three-dimensional structure (position and orientation) of objects in the canopy. In the microwave domain (λ 0.1 to 50 cm), scattering is controlled by the size and orientation of larger objects in the canopy (linear dimensions $>> \lambda$) and soil roughness; absorption is dominated by moisture content. As a result of these different scattering processes optical and microwave models of canopy scattering have generally developed independently (Sun & Ranson, 1995; Lang et al., 1994; Sun et al., 1991; Ulaby et al., 1986). Both optical and microwave scattering models can also be inverted against observations in an effort to derive model parameter estimates (Goel and Strebel, 1983; Kimes et al., 2000, 1997; Pinty & Verstraete, 1991; Weiss et al., 2000). However, the differing nature of the models in the two wavelength domains has led to inversion methods being applied independently to optical and microwave observations rather than in combination (Ranson et al., 1997).

Much less has been done on exploiting microwave scattering models in parameter retrieval. However, there are some interesting recent examples showing how this can be done. Moghaddam and Saatchi (1995) have validated a radiative transfer model by comparing simulations for AIRSAR (C-, L- and P-band) signatures of young- and old-Jack Pine. They have then replaced the model with polynomial fits (dependent on the canopy permittivity) to provide an estimation algorithm for tree moisture (Moghaddam & Saatchi, 1999). They have gone further and used a quasi-radiative transfer model to derive both canopy and stem water content, and thence biomass (Saatchi & Moghaddam, 2000) by fitting some of the more complicated canopy structural parameters against AIRSAR data. Lin and Sarabandi (1999a,b) have also used a linearised form of their coherent scattering model, by showing first that it reproduces both C- and L-band backscattering and interferometric signatures for a forest stand, and then generating linear fits in parameter space, *locally* around the validation. Some alternative approaches have exploited artificial neural networks to solve similar problems by first training the network using model simulations (Kimes et al., 1997; Pierce et al., 1995) and then testing the resulting networks for deriving forest characteristics using real data. Kimes et al. (1998) review methods that include both optical and radar data and models.

If the 3D structure of a particular canopy can be described explicitly then it is possible to use models of canopy scattering behaviour to describe the radiometric response of such a canopy in both the microwave and optical domains. Such model simulations can be used to explore the impact of canopy structure on the EO signal as well as for generating look-up-tables (LUTs) of canopy response in the optical and microwave domains. In this way estimates of biophysical parameters of importance for studies of the carbon cycle and global climate, such as leaf area index (LAI), biomass and canopy cover can be generated from combined optical and microwave EO data. The potential of 3D structural modelling to provide a framework for combining optical and microwave data has important implications for improving biophysical parameter information retrieval from EO data.

Many approaches to modelling 3D canopy architecture have been developed with particular emphasis in recent years in morphogenetic and functional–structural modelling i.e. linking genetic and process-based aspects of tree growth to development of plant structure (Mêch & Prusinkiewicz, 1996; Perttunen et al., 1996; Reffye et al., 1997; Sievanen et al., 2000). Godin and Sinoquet (2005) review current developments in these research areas.

However, such representations are typically used for detailed process-level simulation of canopy response to environmental drivers (climate, availability of water, nutrients etc.) and ecosystem management (Kurth & Sloboda, 1997; Mäkelä et al., 2000; Reffye et al., 1999), rather than for representing how such a canopy might look from EO. In the latter application, only the external properties of a tree contributing to its absorption or scattering of incoming radiation are of interest, as only these can be measured (Disney et al., 2004; Lewis et al., 2004). In studies where the EO signal has been examined, this has generally been for a particular species type and sensor and/or using simplified structural and/or scattering models (Courbaud et al., 2003; Proisy et al., 2002). This paper describes an approach that is essentially generic: given a description of a 3D canopy of arbitrary complexity derived from models or measurements or both, along with radiometric properties of canopy components, the canopy radiation regime can be simulated in the optical and microwave domains using the same structural description.

As a demonstration of this method, this paper presents a structural and radiometric comparison of a modeled Scots pine canopy with observations. Forest structure is compared with ground-based measurements of tree height and trunk diameter-at-breast-height (dbh). Canopy reflectance (ρ_{canopy}) and backscatter (σ) are simulated and compared with data collected during the Synthetic Aperture RADAR and Hyperspectral Airborne Campaign (SHAC) over Thetford Forest, Norfolk, UK in 2000 (Saich et al., 2001; http://www.neodc.rl.ac.uk/index.php?option=displaypage&Itemid=66&op=page&SubMenu=66; Balzter et al., 2001). The utility of the 3D structural approach to modelling scattering in both the optical and microwave domains is explored and implications discussed. In this paper we establish the utility of the forward modelling approach. We do not solve the inverse problem as there are a number of issues raised by this which will be discussed in detail elsewhere. Detailed examination of the scattering behaviour within the modeled canopy and some implications for parameter retrieval via inversion are presented in Saich et al. (2003).

2. Material and methods

2.1. Scattering models

The aim of constructing 3D models of canopy structure in this case is to develop a robust method for simulating the canopy radiation regime in the optical and microwave domains using the fewest assumptions possible. This requires development of a credible model of forest canopy structure which can then be combined with radiation scattering models. The models used for simulating canopy radiometric response were *drat* (aDvanced Radiometric rAy Tracer) in the optical domain and CASM (Coherent Additive Scattering Model) in the microwave domain.

The *drat* model is an efficient Monte Carlo ray tracing (MCRT) model (Disney et al., 2000; Lewis, 1999), which is driven by 3D locations and orientations of scattering elements (including triangles, spheres, cylinders, spheroids, ellipsoids, Bezier patches etc.) combined with descriptions of radiometric properties of the primitive set (reflectance, transmittance at specified wavelengths) (Saich et al., 2003). This model has been used in a number of simulation studies and has been shown to agree with both measurements and other models of canopy scattering (Liang, 2004; Pinty et al., 2004). A highly efficient scattering model is required given that each 3D Scots pine tree model contains of the order 10^7 scattering primitives and a modelled forest stand may contain several thousand trees, resulting in potentially $>10^{10}$ primitives in a large scene.

The CASM model is a (coherent) single scattering model of microwave backscatter, also driven by canopy geometry. The model is very similar to that of Lin and Sarabandi (1999a,b) in which backscattered power is calculated by direct summation of the far-field scattering from an ensemble of N particles with positions r_p. In this case

$$\sigma = \frac{4\pi}{A}\langle \bar{F}\bar{F}^{*}\rangle \tag{1}$$

where A is the illuminated area and

$$\bar{F} = \sum_{p=1}^{p=N} \bar{f}^{(p)} e^{ik\left(\hat{\mathbf{k}}_s - \hat{\mathbf{k}}_i\right)\cdot \bar{r}_p} = \sum_{p=1}^{p=N} \bar{f}^{(p)} e^{-2ik\hat{\mathbf{k}}_i \cdot \bar{r}_p} \tag{2}$$

Here k is the propagation constant, $\bar{f}^{(p)}$ is the scattering amplitude of the pth particle, $\bar{F}$ is the total electric field (ignoring the far-field Green's function term), $\bar{F}^{*}$ is the complex conjugate of $\bar{F}$, and we have assumed backscattering ($k_s = -k_i$). The components of the trees are modelled as finite cylinders, based on the use of the internal field of an infinite cylinder (Karam and Fung, 1988; Karam et al., 1988). Interactions with the ground are also included for paths that scatter from the vegetation to the ground and then the sensor and vice versa. Within this implementation, a multiplicative factor has been included to take account of the effects of the surface roughness of the ground in lowering the reflected power, so that the Fresnel coefficient is replaced with

$$\bar{g} = \bar{r}\, e^{-2(k_0 s\cos\theta)^2} \tag{3}$$

where the standard deviation in vertical height is s, $\bar{r}$ is the Fresnel reflection coefficient and θ is the scattering angle. The permittivity of the ground surface is related to the soil moisture via the empirical relationship of Hallikainen et al. (1985).

To take account of extinction losses in the medium, Foldy's approximation (Tsang et al., 1985) is used to derive the effective propagation constant. A three-dimensional grid is implemented to allow representation of both vertical and horizontal inhomogeneity in the vegetation canopy. Propagation constants are determined on a cell-by-cell basis. Full details of the model configuration are given in Saich et al. (2003).

2.2. Canopy structural representation

The representation of canopy structure used in this study was provided by the Treegrow model developed by Leersnijder (1992). Treegrow is an empirical growth model which is parameterised by species-dependent branching statistics in conjunction with specified external environmental conditions such as the available light regime to simulate individual tree development with time. The model has been used previously by Woodhouse and Hoekman (2000) for example to generate statistical properties of an ensemble of scattering objects for simulation of RADAR backscatter from conifer canopies. Whilst this approach is suitable for driving backscatter models which approximate forest structure as layers of simple scattering objects (e.g. cylinders) much of the fine-scale 3D structural information output by Treegrow is not used. The use of a coherent scattering model such as CASM permits full use of the detailed 3D structural models and requires locations of the individual scattering elements to be defined. This detailed structural information becomes important when simulating radiation in the optical domain where wavelength is much less than the dimensions of the canopy scattering elements, even needles (not the case at microwave wavelengths).

The Treegrow model is driven by:

1. Environmental parameters: the availability of photosynthetically active radiation (PAR) at the bottom of the crown.
2. Species specific parameters: number of shoot types; maximum number of flushes per year; number of shoot orders; minimum shoot length; maximum age of shoots with leaves; maximum stagnation time of a shoot; maximum tolerable light reduction (%).
3. Tree specific parameters: an empirical canopy height function; height to crown; maximum crown radius; maximum length of main stem.

Given these various parameters the model will "grow" a tree to a specified age in specified time increments (a single year being the smallest time step), following the various limiting and controlling functions. In this study, if no information regarding a specific parameter was available default parameters were used (see Appendix A for full list of default Treegrow parameters). As far as possible, parameters

were modified in order that the 3D structural information output by the structural model matched observed structural information. This is described below.

2.3. Tree height and diameter-at-breast-height (dbh)

The tree height increment described by Treegrow is controlled by two factors: the light reduction environment within the canopy, and a species- and site-specific empirical height function. The former property requires the definition of a (arbitrary) light reduction function within the canopy. This function describes the variation with age of the percentage of light reaching the ground from the top of the canopy and primarily controls the crown shape. It is in the definition of the light reduction function that a limitation of the stand-based parameterisation of the model becomes apparent. The default light reduction behaviour is based on observations made in a stand that has undergone extensive thinning at various times and this is manifested as severe "saw-tooth" variations in light reduction with time from age 15 years onwards. This behaviour (and the longer term trend of gradual reduction in light penetrating the crown and reaching the ground) results in modelled tree height actually reducing with increasing time beyond a certain age and with a crown shape markedly different from that observed at Thetford. This is a result of the Treegrow model parameterisations having been based on stand-averaged measurements. In such a case it is reasonable that a thinned stand, with the tallest trees having been felled, may reduce in (average) height with age and develop a different crown shape than would be the case in the absence of thinning. This is clearly not valid when applied to an individual tree, so in this study a modified light reduction function more applicable to individual trees in a stand is developed. This makes the assumption that a function generated from stand-averaged light extinction behaviour can in fact represent the light extinction environment of individual trees, but only if trees within a stand are relatively homogeneous. The more heterogeneous the stand, the less valid such a relationship will be. However, in stands such as those at Thetford used in this study the trees are planted in an extremely regular pattern and are thinned to optimise growth conditions for all trees in a stand. As a result, trees in a given stand have a similar structure suggesting it is reasonable to assume that trees of a particular age will have similar light extinction environments and hence structural development. This is not the case for natural stands, where light extinction environments differ drastically between trees according to age and proximity of competing individuals (amongst other factors). The modified light reduction function used here was estimated iteratively by simulating the light reduction through tree crowns generated with the default light reduction function, comparing resultant modelled and observed tree heights (and crown shape), updating the function and then re-simulating. The default Treegrow and modified light reduction functions are shown in Fig. 1.

It can be seen from Fig. 1 that significant change in the default Treegrow light reduction behaviour is required in order to match modelled to observed tree height. However, the extreme thinning stages included in Treegrow parameterisation are not realistic for trees at Thetford, where thinning is far more gradual until harvest (*pers. comm.* Dr. Sebastien Lafont, formerly UK Forest Research, Alice Holt, now ECMWF). For this study, modelled trees were only generated to age 50 years as this corresponds with the region of maximum canopy growth. Beyond age 50, annual increments in canopy structure become smaller and smaller and so are less likely to influence the measured ρ_{canopy} and σ signal against which any comparison of modelled response is performed.

Fig. 2(a) shows a comparison of tree height values modelled using the original and modified light reduction curve with heights based on measurements made during the SHAC

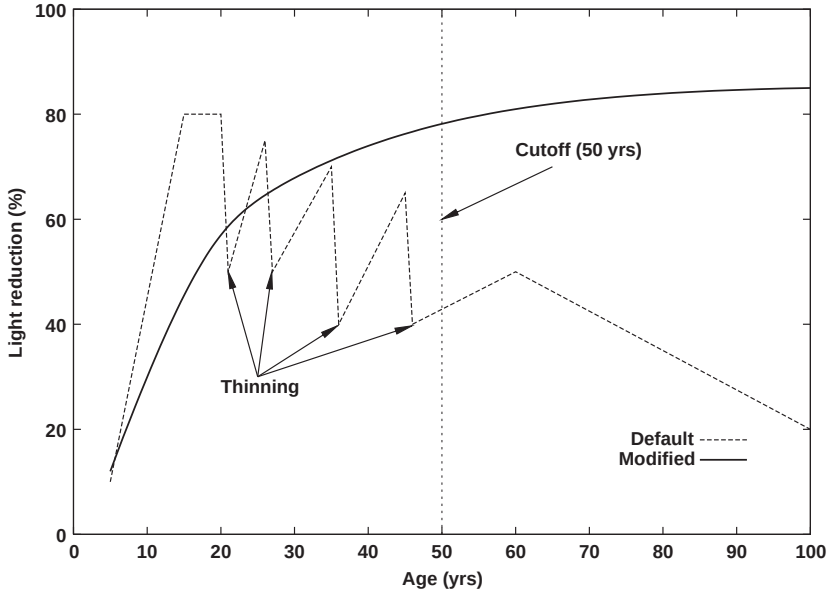

Fig. 1. Default and modified light reduction curves used in Treegrow model to generate 3D canopy structural information for Scots pine.

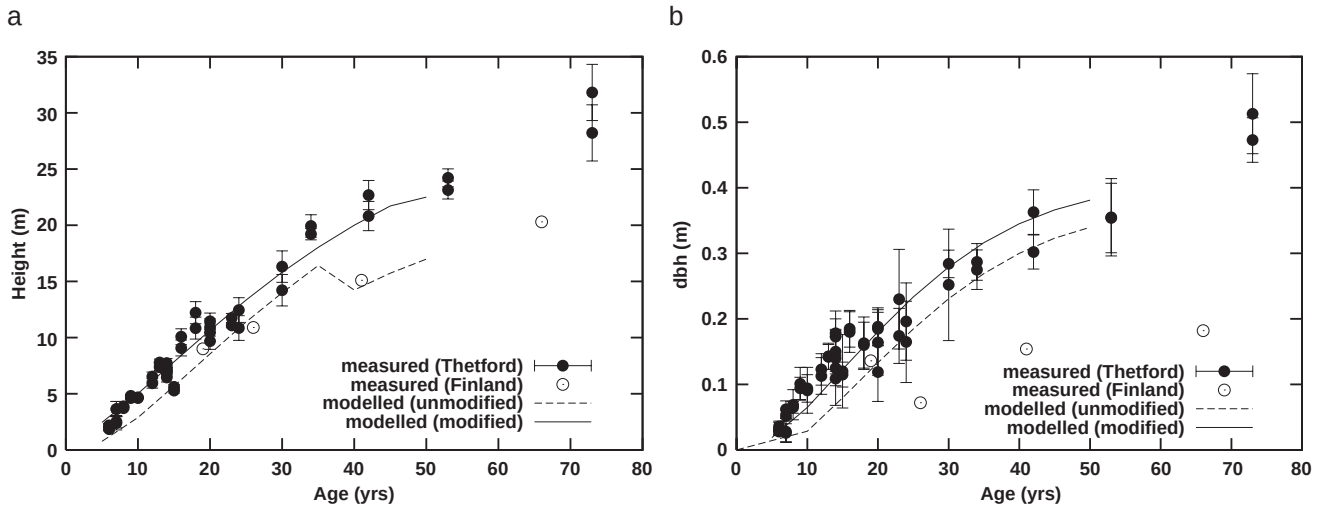

Fig. 2. a) Tree height (modelled using default light reduction curve) against tree height measured in Thetford Forest and Finland, as a function of tree age; b) as for (a) but for dbh.

campaign (Balzter et al., 2001; Saich et al., 2001). In this case, tree heights from a Finnish Scots pine stand[1] are also included for comparison as the Treegrow model was originally parameterised using measurements made in Finland. These measurements illustrate the difference the light and management regimes can have on tree growth. The variation of modelled height values at each age represents the variation in tree structure as a result of changing the random seed during generation of each tree. Changing the seed value introduces a stochastic element to what is essentially a deterministic model and allows for variation in a population of statistically similar trees generated by the model in order to mimic observed variability.

It can be seen from Fig. 2(a) that the tree heights modelled using the default light reduction function are in reasonable agreement with the measurements (modelled height is slightly too low) until about age 30 years. After this stage the modelled tree height reduces, for the reasons described above, before rising again. The tree heights modelled with the modified light reduction function show that the anomalous reduction in modelled tree height has been removed. The agreement between modelled tree height and measurements made in Thetford in this case is extremely close (r^2 value of 0.96). The agreement with the Finnish tree height values is also good until about 25 or 30 years of age but after this the Finnish trees are substantially smaller than those of equivalent age at Thetford. Interestingly, the Treegrow model was based on measurements made in Finnish Scots pine stands and this is reflected in the fact that the default model behaviour changes after age 35 to follow the Finnish observations much more closely. This is partially due to different growth conditions (different latitudes and climate) but also as a result of the thinning practices applied in the Finnish stand being substantially different from those applied in Thetford significantly reducing the overall mean height of the tree stand at certain ages.

[1] We are grateful for data provided by Risto Sievenan, Finnish Forest Research Institute (METLA), Vantaa Unit, PL 18, 01301 Vantaa.

Diameter-at-breast-height (dbh) was used as a further comparison of measured and modelled structural parameters. Dbh describes the trunk diameter at a height of 1.3 m from the ground. This measure is used as it is relatively simple to make and can be related to tree height and/or trunk size. As a result it is often used as a driving parameter for microwave scattering models of vegetation, where the size (and scattering properties) of the trunk has a major impact on scattering behaviour. Fig. 2(b) shows the comparison of measured against modelled dbh for the Thetford Forests and Finnish sites. Unsurprisingly, the trend is very similar to that observed for height although there is far greater variability within age-stands in this case. Values of dbh range from a few centimeters in early growth stages to 0.35 m at age 50 years. Again, the Finnish forest is notably smaller after age 20 or so than the Thetford case as trees with larger dbh are likely to be selected preferentially because of their greater timber yield (per tree felled). Agreement between measured and modelled dbh is shown by an r^2 value of 0.97.

In addition to the light environment describe above, which has an indirect impact on modelled tree height, Treegrow also uses an empirical (species-specific) function to describe tree height with age (which is modulated by the light environment). Tree height at time t, h_t, is governed by Eq. (4):

$$h_t = S\left[1 - e^{(-H_1 t)}\right]^{H_2} + [H_3 h_{t-1}] \quad (4)$$

where H_1, H_2 and H_3 are empirical parameters controlling the rate of increase, amplitude and decay of the annual height increment $\Delta h_t = (h_t - h_{t-1})$; S is a constant (30); h_{t-1} is the height at the previous time step, $t-1$. The default values of H_1, H_2 and H_3 are 0.035, 1.8 and 0.2, respectively, resulting in a function of Δh which increases rapidly, to a maximum of 0.4 m yr^{-1} after 17 years, before decaying gradually. Values of $H_{1,2,3}$ parameters were generated for the Thetford stands by fitting a function of the form of Eq. (4) to the observed height measurements shown in Fig. 2. Resulting values of $H_{1,2,3}$ were 0.05, 2 and 0.22, respectively. Fig. 3 shows the measured values of tree height h, as well as the unmodified and modified

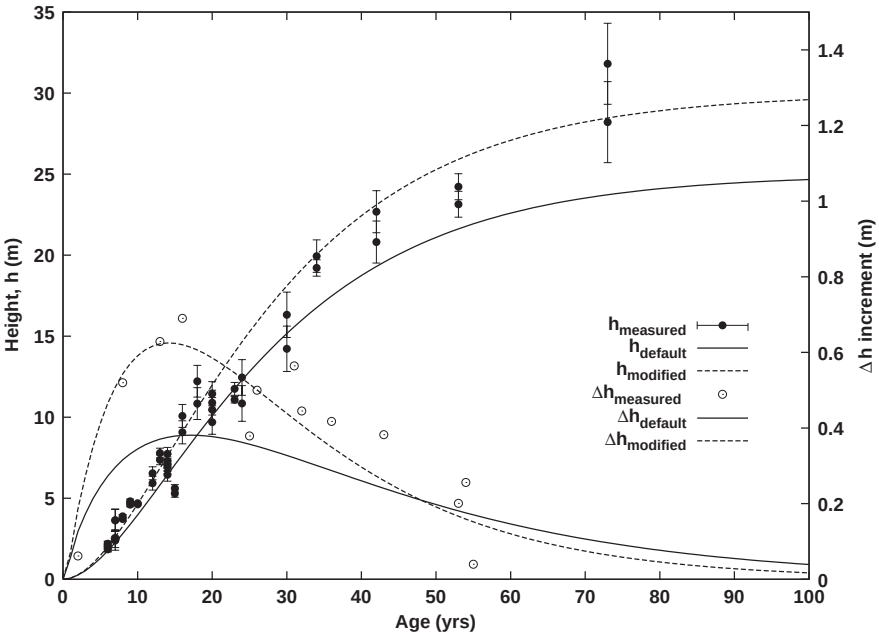

Fig. 3. Measured tree height h ($\pm 1\sigma$, left axis) with age, from Thetford Forest (filled circles) compared with h modelled using the Treegrow default and modified h functions (solid and dotted lines, respectively). Also shown are the corresponding height increment values, Δh, ($\pm 1\sigma$, right axis) for measured h (open circles) and the default and modified h functions (solid and dotted lines, respectively).

Treegrow height functions based on the derived values of $H_{1,2,3}$. Also shown in Fig. 3 are the values of Δh_t derived from measured h, as well as the unmodified and modified model values of Δh_t derived by transforming Eq. (4).

It can be seen from Fig. 3 that although the form of Eq. (4) follows measurements of h, the unmodified function tends to underestimate the observed values of h with age, whereas the modified function fits the observations far more closely. This is reflected in r^2 values of 0.95 compared to 0.98. This illustrates the improved model representation of tree height for the Thetford Scots pine trees. The progression of Δh_t with age in Fig. 3 is less clear cut as a result of the variability of observed h. There is an obvious peak in measured Δh_t at around 15 years but there is also a high level of variability. This is reflected in the values of Δh_t calculated from the modified height function.

2.4. Generation of forest stands

Using the modified light reduction function described above along with default values of other structural parameters (height to crown, maximum height of main stem, maximum crown radius) a series of trees were generated. Rather than generate a forest stand by 'cloning' the same tree many times over, a number of individual trees were generated at each age stage by re-seeding the pseudo-random number generator used to sample pre-defined probability distributions. This permits some tree-level variability within each age group (as seen in Fig. 2). Fig. 4 shows the development of an individual modelled Scots pine tree with age from 5 to 50 years. For comparison, Fig. 5 shows a Scots pine stand of age 34 years in Thetford Forest.

In order to create model forest stands, individual trees were distributed according to a specified tree density, with "cloned" instances of a particular tree being randomly selected and rotated in azimuth within the modelled stand (Disney et al., 2000). The modelled forest stands were generated to be 300 m on a side (to avoid edge effects only the central 50 by 50 m region is viewed in simulations). Tree spacing was varied from 1.5 to 6 m in both horizontal dimensions. These spacings were based on measurements made by UK Forestry Research workers in Thetford Forest (*pers. comm.* Dr. Sebastien Lafont). Juvenile trees are planted with a spacing of around 1.5–2 m but the spacing grows to around 4 or 5 m as the trees mature and the stands are thinned out. Random variability of up to 0.75 m was included in the spacing used in the generation of forest stands to take account of variability estimated from photographs taken during the SHAC 2000 campaign.

Fig. 6 (left-hand axis) shows the variation of stand LAI (total one-sided green needle area divided by total stand area) as a result of the density variations discussed above. There is (unsurprisingly) a wide range of variation LAI with planting density, ranging from 2.5 to 20 for the high and low density stands respectively at age 5 years. Apart from the densest stands, LAI is relatively constant with age: the amount of green needle area does not vary anywhere near as much as the tree height. Trees at age 50 years have similar amounts of needles to their younger counterparts, but with far larger trunks. LAI can actually fall as the canopy gets taller and broader, while adding little green needle material. As a result of this behaviour, combined with the effect of thinning, the true stand LAI will not follow any one of the trajectories shown in Fig. 6 but will start at the high end at age 5 years (spacing closer to 1.5 m line) and progress to the lower end (spacing closer to 6 m) at age 50 years. Fig. 6 also shows (right-hand axis) how the mean measured tree spacing ($\pm 1\sigma$) of canopies increases in near-linear fashion with age after 20 years, from the first major thinning.

Fig. 4. Development of a Scots pine tree based on modified Treegrow output for ages 5, 10, 20, 30, 40, 50 years (left to right). The scene reflectance was simulated with the *drat* optical model at a wavelength of 850 nm.

Fig. 5. 34-year old Scots pine stand at Thetford Forest (photograph by P. Saich).

2.5. Needle properties

Forest scattering behaviour, in the optical domain in particular, is not only a function of canopy density but also of the size and arrangement of needles on the tree (Cermák et al., 1998; Cescattti, 1998; Stenberg et al., 2001). Needles influence the (optical) radiometric behaviour of the canopy through (amongst other things) absorption of photosynthetically active radiation (PAR, $\lambda = 0.4–0.7$ μm) and this behaviour will be related to their number, orientation and distribution. Smolander and Stenberg (2003) have, for example, shown the impact of needle clumping on the angular variation of reflectance behaviour in simplified mathematical radiative transfer models of optical ρ_{canopy}. Specifically, they showed that the use of empirical clumping parameters used to simplify radiative transfer models of canopy scattering can introduce significant underestimation of intercepted PAR for given LAI due to underestimated multiple scattering interactions between needles. They propose a wavelength-independent (i.e. structural only) correction to account for needle clumping more satisfactorily. This correction acts to produce a wavelength-dependent reduction in conifer ρ_{canopy} compared with uncorrected models with the same LAI. Smolander and Stenberg (2005) and Rautiainen and Stenberg (2005) show parameterisations and applications of this approach.

A major advantage of using the 3D approach to modelling conifer ρ_{canopy} as in this study, rather than using approximate

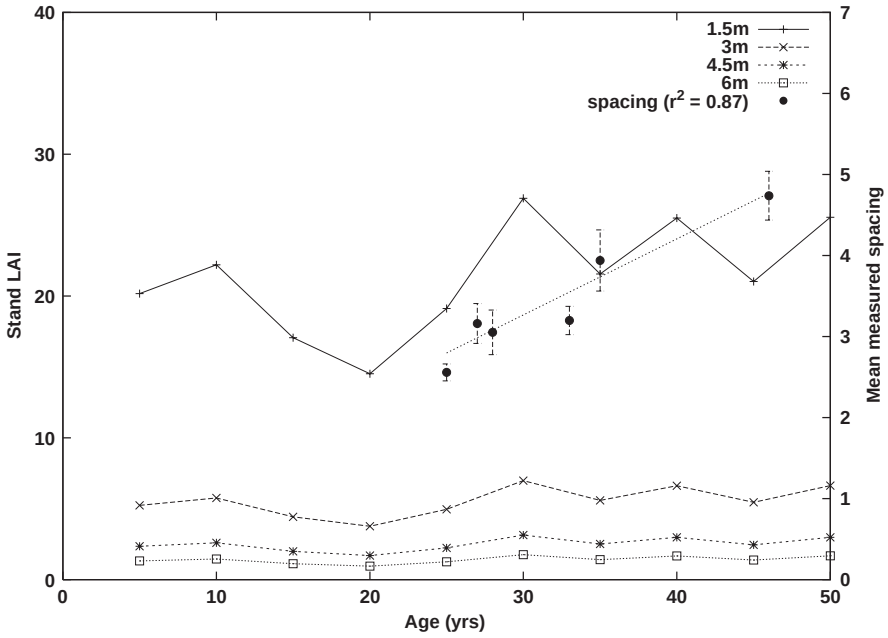

Fig. 6. Stand LAI with age for modelled stands with varying tree spacing (left-hand axis), and mean measured spacing with age ($\pm 1\sigma$, right-hand axis).

radiative transfer models, is that such clumping need not be "corrected" for at all. In fact, the existence of wavelength-independent structural terms as noted by Smolander and Stenberg (2003) which capture the impact of clumping on scattering, may be a useful source of information. Theoretical treatments of the wavelength-independent (structural) canopy terms have been advanced by Panferov et al. (2001) and Knyazikhin et al. (2005). These descriptions are based on the consideration of the recollision probability of photons following interaction with scattering elements within a canopy. These approaches appear promising in practice (Wang et al., 2003). Wavelength-invariant scattering properties of the models presented in this study are explored by Saich et al. (2003). Disney et al. (2005) show that it is possible to nest expressions of leaf/needle scattering based on the approach described by Knyazikhin et al. (2005), within descriptions of ρ_{canopy} derived in the same way. This 'lumped parameter', nested, wavelength-independent approach appears to describe observed ρ_{canopy} accurately in many cases and may be used to derive canopy structural and/or absorption properties from EO data. The expressions of ρ_{canopy} are simple functions of wavelength-independent canopy structural terms, combined with radiometric absorption terms only.

The Treegrow model indicates on which branch order needles will be found but does not describe the location or distribution of needles themselves. For use within the *drat* optical model the needle distribution pattern (phyllotaxy) describes the arrangement of needle pairs (in the case of Scots pine) around the circumference of a given branch. The size and arrangement are parameterised by: needle length; major and minor radii of the ellipsoid; needle normal; angle between needles in a pair; needle density (strictly, needles per unit length). The phyllotaxy is parameterised by specifying the ratio of the number of needle pairs to the number of turns around the branch e.g. phyllotaxy of 26 : 10 would generate 26 pairs of needles for every 10 rotations around the branch. In contrast, Smolander and Stenberg (2003) have used a Fiobnacci sequence to describe the phyllotactic arrangement, based on the study of Cannell and Bowler (1978), with a divergence angle of $8/13 \times 2\pi$ between successive needle pairs and a fascicle angle (defined as the opening angle between needle pairs in a fascicle) uniformly distributed between 0 and $2/13\pi$.

The dimensions of individual needles used in this study follow those published by Smolander and Stenberg (2003) but modified for the particular trees observed in Thetford Forest. Specifically, needle density varies between 25 and 30 cm^{-1}, mean needle length is 3 cm, needle angle from twig is 45° and needle diameter is 0.1 cm. The fascicle angle was fixed at 25°. These are close to the values chosen by Smolander and Stenberg (2003) who used needle angle 40.5°, needle length and diameter of 2.85 and 0.092 cm, respectively, and an equivalent needle density of 25 cm^{-1}. In this study, needles were chosen to be ellipsoidal with cross-sectional radii of 0.1 and 0.05 cm, respectively, i.e. the needles are flatter in one axis than another. Needles are oriented in relation to the twig in such a way that the normal to the upper surface of the flat side is directed towards the axis of the twig. Needles are assumed to be reflecting only and are assumed to have Lambertian scattering surfaces. High values of measured needle reflectance suggest transmittance will be low, suggesting the first assumption is not too drastic (Hosgood et al., 1995). The needle surface is quite dull, so although not precisely Lambertian, there will be little or no specular component.

The impact of needle length, shape and phyllotaxy on simulated forest reflectance was investigated. The needle shape and in particular the ratio of the two cross-sectional radii of the needle ellipsoid were found to have the most significant impact on reflectance. In comparison, needle phyllotaxy and length

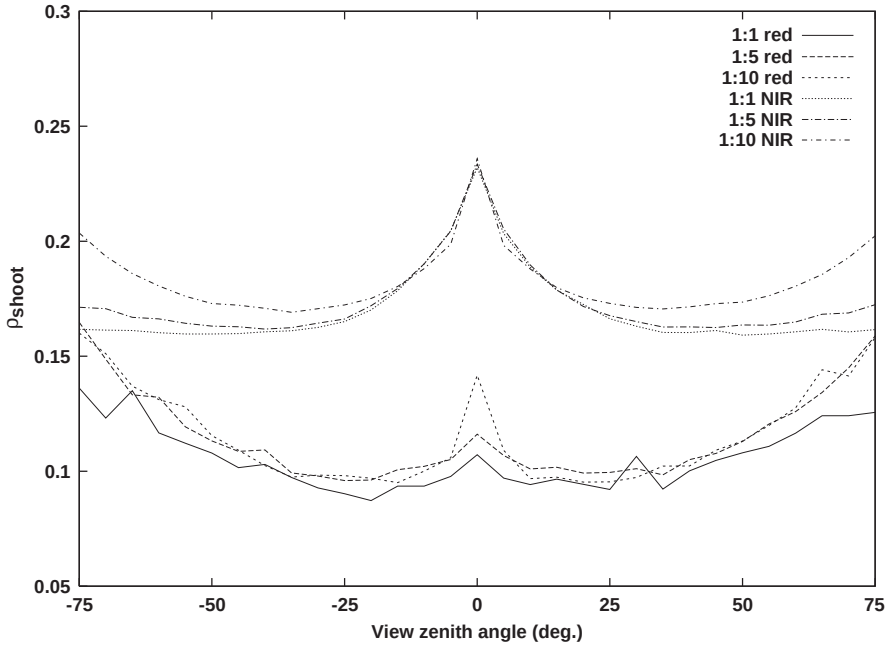

Fig. 7. Variation of angular reflectance of shoot at two wavebands (red = 546 nm, NIR = 844 nm) with the ratio of cross-sectional semi-minor to semi-major axis of the ellipsoidal primitives used to represent needles (1 : 1 is a needle with circular cross section, 1 : 5 represents a flattened ellipsoid; 1 : 10 represents a severely flattened ellipsoid; viewer and illumination at 0° and shoot is viewed/illuminated from bud along axis of shoot).

had relatively small impact on simulated ρ_{canopy}. Fig. 7 illustrates the change in reflectance of a single shoot with the changing ratio of cross-sectional radii. This is expressed in Fig. 7 as the ratio of the radius perpendicular to the upper surface of the needle (as defined above) to the orthogonal radius.

Fig. 7 shows the increase in reflectance as the needle shape progresses from near-cylindrical (1 : 1) to a much flatter shape (10 : 1). At nadir viewing and illumination, there is a clear increase in ρ_{shoot} in the visible red (450 nm) and NIR (850 nm) wavelengths as the needle shape becomes flatter. The effect of needle shape is seen in the reduced limb-brightening with increased flattening observed in the NIR. This is a result of the particular needle configuration: the flatter the needle shape, the more the scattering phase function of the needles exhibits a preferential scattering direction. The scattering behaviour away from the hotspot region (nadir in this case) is significantly different for the different needle shapes.

Stenberg et al. (2001) define a quantity $\overline{STAR}$, the spherically averaged shoot silhouette to total area ratio (Oker-Blom & Smolander, 1988; Stenberg et al., 2001). This is defined in Eq. (5) and describes the projected area of the shoot over all angles as a fraction of the total area.

$$\overline{STAR} = \frac{1}{\text{TNA}} \frac{1}{4\pi} \int_{4\pi} \text{SSA}(\boldsymbol{\Omega}) \text{d}\boldsymbol{\Omega} \tag{5}$$

where TNA is the total needle area; $\boldsymbol{\Omega}$ is the viewing vector, and is a function of view zenith (θ) and azimuth (ϕ) angles.

A shoot of the same length as that of Smolander and Stenberg (2003) was constructed. Using the phyllotaxy described above, needles of the same length and cross-sectional radii as those of Smolander and Stenberg (2003) were added (but ellipsoidal rather than cylindrical) and $\overline{STAR}$ values were calculated for the resulting shoot by MCRT simulation. Results for both shoots are compared in Table 1 (SS: Smolander & Stenberg, 2003; DLS: Disney, Lewis and Saich, this study). Fig. 8 shows a comparison of the SS and DLS shoots (prior to implementation of Fibonacci sequence) from nadir and 45°.

Results in Table 1 show that the SS shoot has a higher area (156.5 cm^2) than the equivalent DLS(a) case (107.9 cm^2) for a given number of needles of fixed size. This is a result of the larger area of a cylinder of length l and cross-sectional radius r compared with the equivalent ellipsoid of major radius $l/2$ and minor radii r. Interestingly, $\overline{STAR}$ for the (default) case (0.225) is somewhat higher than for the SS case as a result of the flattened ellipsoidal shape of the needles affecting the mean needle area. In this case, needle orientation is significant. The DLS(a) scenario represents a shoot with the same phyllotaxy as that of the default case but with needles of the same dimensions as the SS case. In this scenario both minor radii are equal i.e. needles are prolate (elongated) spheroids rather than cylindri-

Table 1
Comparison of STAR values for shoots used by Smolander and Stenberg (2003) (SS) and those used in this study (DLS)

	SS	DLS (default)	DLS (a)	DLS (b)
No. of needles	190	166	220	198
Needle length	2.85 cm	3.0 cm	2.85 cm	3.2 cm
Cross section (diameter)	0.092 cm	0.1, 0.2 cm	0.092, 0.092 cm	0.05, 0.05 cm
Single needle area	0.824 cm^2	1.14 cm^2	0.65 cm^2	0.79 cm^2
Total needle area	156.5 cm^2	190.2 cm^2	142.6 cm^2	156.4 cm^2
$\overline{STAR}$	0.133	0.225	0.231	0.201

DLS (default) are values used in later simulations; DLS(a) scenario matches needle dimensions of SS case; DLS(b) matches needle area of SS case (modified needle phyllotaxy and needle dimensions).

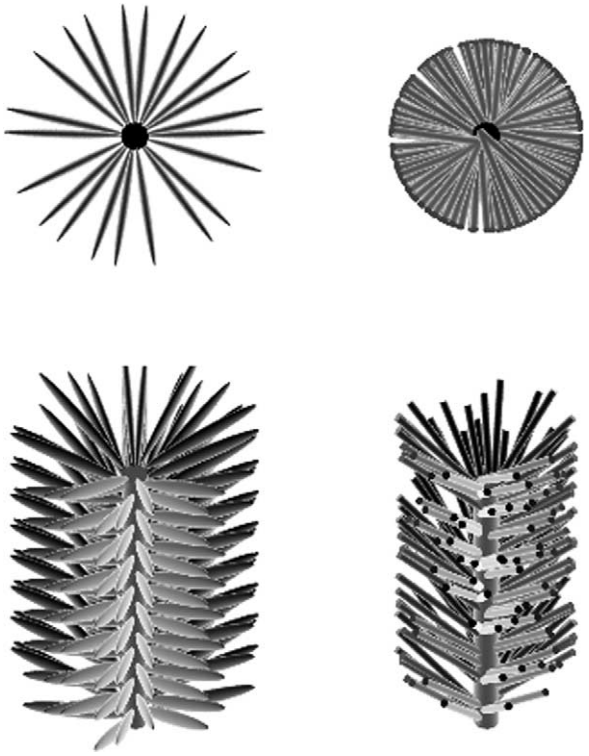

Fig. 8. Two shoot designs: top row is nadir and bottom row is 45° viewing zenith angles: left: DLS (Disney Lewis Saich) representation (this paper, prior to imposition of Fibonacci distribution); right: Smolander and Stenberg (2003) (SS).

cal, but not flattened. In this case, many more needles are included in order to match the same needle density, yet the total area is still lower than the SS case. Unsurprisingly, the $\overline{STAR}$ increases to 0.231. The DLS(b) scenario is the closest match of total SS needle area and needle number under the specified phyllotaxy and needle length. In this case, needle diameter must be reduced significantly and the resulting $\overline{STAR}$ falls to 0.201 due to the smaller number of needles with less preferential angular scattering. Clearly, phyllotaxy and needle shape can have a significant impact on scattering behaviour. The use of a phyllotactic arrangement for needles based on a Fibonacci sequence (as in Smolander & Stenberg, 2003) provides significant benefits. In particular, it is more closely based on observation and has evolved to maximise available area for light interception by minimising self-shadowing (this effect is obvious from the nadir views in Fig. 8). As a result, the Fibonacci-based distribution was subsequently implemented for the models used in this study.

Choice of needle shape is also important. As a consequence of assuming Lambertian scattering, needles tending to a more cylindrical shape scatter far less radiation than might be expected for a given size. A flatter needle shape resulted in far higher values of $\overline{STAR}$ for a given LAI (or needle area in this case). The strong impact of needle shape on simulated ρ_{canopy} indicates that care should be taken over selecting an appropriate form. In particular, the selection of needle shapes as cylindrical may not be appropriate, particularly if surface reflectance is Lambertian (leading to significant underestimation of the scattering phase function) and transmittance is ignored. Fig. 9 demonstrates the impact of needle shape and phyllotaxy on multiple scattering behaviour (assuming no transmittance and direct illumination only). This dependence on shape is a further advantage of using a model which allows for explicit descriptions of needle shape, size and location.

For both the DLS and SS shoots, the contribution to the signal is seen to drop off very rapidly after the first scattering

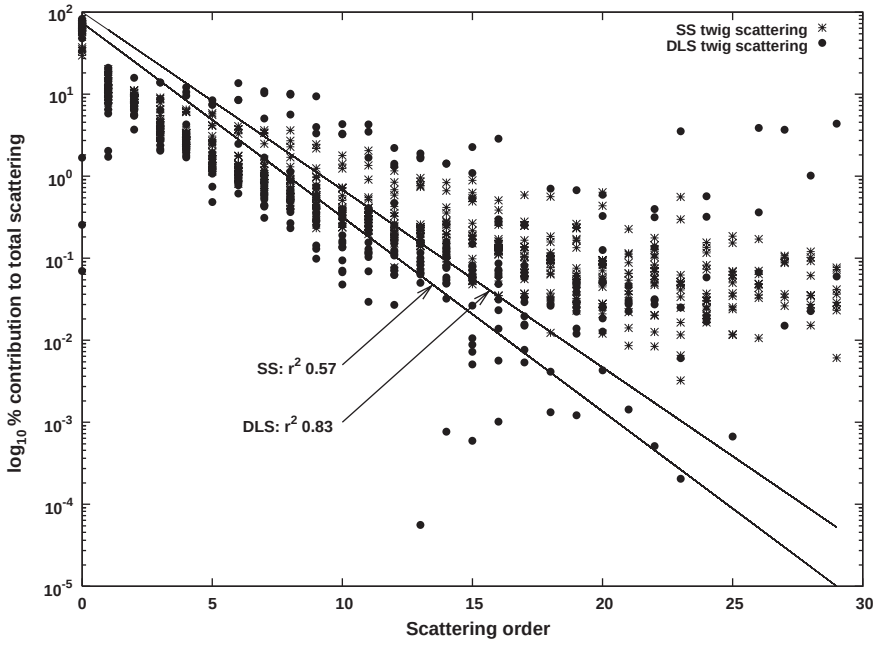

Fig. 9. Log_{10} % contribution to total scattering as a function of scattering order (number of interactions) for the default DLS and SS shoot/needle configurations.

contribution (scattering order 1). In Fig. 9 all view zenith angles are lumped together but the variation of contribution with view zenith angle can be seen in the range of values for each scattering order. For the SS shoot, at high view zenith angles (−85°, 85°) the single scattering contribution is of the order of 30% of the total, with the contributions falling below 1% at around scattering order 10. For the nadir case, the single scattering contribution is 76%, falling to below 1% after only 5 scattering interactions. The DLS shoot shows significantly different behaviour, with single scattering at high view zenith angles being <5% of the total. The contributions fall off far more slowly with scattering order compared with the SS shoot to the extent that contributions do not fall consistently below 1% until >25 scattering interactions. The nadir case for the DLS shoot however shows similar behaviour to the SS shoot, with a single scattering contribution of 83% falling to below 1% at scattering order 5. The regression lines in Fig. 9 also indicate that multiple scattering behaviour of the SS shoot configuration is far more variable than the DLS case (r^2 of 0.57 compared with 0.83) with the multiple scattering contribution dropping off more rapidly than for the DLS shoot. Fig. 9 illustrates the impact of needle shape and phyllotaxy on multiple scattering behaviour (particularly as a function of view/illumination angle) at the shoot-scale.

2.6. Trunk, bark and needle properties

The trunk/bark reflectance used in the optical model simulations was a laboratory-measured spectrum of bark material, recorded in the European Goniometric Observatory (EGO) facility at JRC, Ispra, Italy, during the LOPEX experiment (Hosgood et al., 1995). For optical forest stand simulations, canopy understory was considered to be a simple Lambertian soil surface. This may also impact simulations significantly as the relatively dense understory vegetation within Thetford can be seen in Fig. 6. However, it is also true that the understory of the denser canopies is dominated by soil and dead needle material only. Soil reflectance values were taken from the soil basis functions of Price (1990), which have been shown to reconstruct 99.6% of observed variance of measured spectra. Needle reflectance was derived from the LIBERTY model (Dawson et al., 1998), modified (*pers. comm* T. Dawson) to accommodate the absorption coefficients derived from the PROSPECT leaf reflectance model (Jacquemoud & Baret, 1990; Jacquemoud et al., 1996). Needle transmittance was assumed to be zero. Clearly this may have an impact on canopy scattering behaviour (particularly multiple scattering in the near infrared) but there appear to be very few published studies of needle transmittance properties.

2.7. HyMAP airborne optical data

HyMAP is an airborne whiskbroom hyperspectral digital scanner developed for a range of commercial remote sensing applications (Cocks et al., 1998). HyMAP data were geometrically corrected and registered to the OSGB36 datum. Atmospheric correction was carried out using HYCORR with continental aerosol model and mid-latitude summer atmospheric profile (Boardman, 1998). The HyMAP data from SHAC 2000 consisted of 126 spectral bands ranging from 437 to 2485.9 nm in steps of 16 nm (bandwidth 10–20 nm). Three flightlines were flown (up and back) on the 17th June 2000 at 10:36 (heading 180°), 10:47 (heading 2°) and 10:59 (heading 181°), at an altitude of 6500 m above ground level. The at-ground spatial resolution from this altitude is around 4 m with a swath width of around 2.5–3 km. Unfortunately the HyMAP flightlines were between 30° and 40° off the solar principle plane and so much of the angular signal, which is at its greatest in the solar principal plane, was missed. This has implications for the model results described below.

2.8. E-SAR airborne synthetic aperture RADAR data

The microwave data used in this study were acquired during the SHAC 2000 campaign over Thetford Forest, 31st May 2000, using the DLR E-SAR instrument (Balzter et al., 2001). Overpasses were made between 09:49 and 11:08, with track angles of −178° (X-band) and 2° (L-band). These data include L-band (HH, VV and HV) backscattered powers, L-band coherence and interferometric height (derived from repeat-pass observations), and X-band interferometric heights. The 4-look products have a spatial resolution of approximately 4 m (range) × 2.5 m (azimuth) and the site was imaged at a range of incident angles between ~40° and 60°. CASM simulations of the Thetford Forest canopy were carried out for fixed vegetation moisture (0.7) and soil moisture (0.1) for canopy ages of 10–50 years every 10 years, with appropriate corresponding tree densities based on in situ measurements.

In each case, thirty pairs of simulations were conducted to generate the interferometric phase and coherence (across all of the simulations). From the simulations the backscattered powers under both the coherent and incoherent summations can be calculated. In any single simulation, a set of five trees was used to populate (with given planting positions) a 300 × 300 m area (as in the optical case), and from this the central 25 × 25 m cell has been taken to form the basis for that simulation. In all cases, the flight altitude is assumed to be 3000 m and the (horizontal) baseline is 10 m.

3. Results

Using the ground data collected during the SHAC campaign 19 stands of Scots pine of age 5 to 53 years were identified within the HyMAP images. These stands and their sizes in pixels are listed in Table 2 (pixel size 4 × 4 m). Stands were also located within the E-SAR data in the same manner, although fewer age stands were covered by the E-SAR instrument.

Several stands of age 5, 10 and close to 15 years exist within the HyMAP data, but fewer of the older stands were covered, including only four in total over the age of 30 years.

Table 2
Scots pine stand ages in HyMAP data, with size in pixels

Stand age (yr)	Stand size (pixels)
5	850
5	1900
5	2208
10	2418
10	2639
10	4218
10	1664
14	1702
16	2898
20	1764
20	6060
20	2808
24	2565
24	2170
30	2964
34	4796
42	946
53	1302
73	350

Rectangular subsets of these stands were extracted and their mean reflectance and variance were calculated. Mean values were used in order to reduce significant intra-stand variability caused by the small size of the stands suitable for extraction from the HyMAP data. Viewing zenith and azimuth angles for each subset were calculated from the aircraft ephemeris data. Solar zenith and azimuth angles were calculated from the time of day and location.

Using the *drat* optical and CASM microwave models described above, ρ_{canopy} and σ were simulated at the viewing/illumination configurations observed within the HyMAP and E-SAR data. The resulting drat-simulated optical reflectance values are shown in Fig. 10 for four spectral bands (446, 544, 646 and 844 nm) along with the corresponding HyMAP reflectance values. Fig. 11a shows a regression of ρ_{measured} against ρ_{modelled}, assuming no specific tree density for a given age in the modelled canopies. In Fig. 11b the regression is carried out assuming the 3 m tree spacing for canopies of age $\leq$20 years, and against the 6 m spacing thereafter.

Fig. 12 shows variation of L- and X-band backscatter values with age simulated over the Thetford Forest stands for varying canopy age. Fig. 13 shows the comparison of measured and modelled microwave backscatter values, for the L-band simulations in the HH, HV and VV polarisations.

Fig. 14a shows a comparison of X-band simulated backscatter with age at two extreme canopy spacings (1 and 20 m) with E-SAR X-band VV polarised observations. Fig. 14b shows

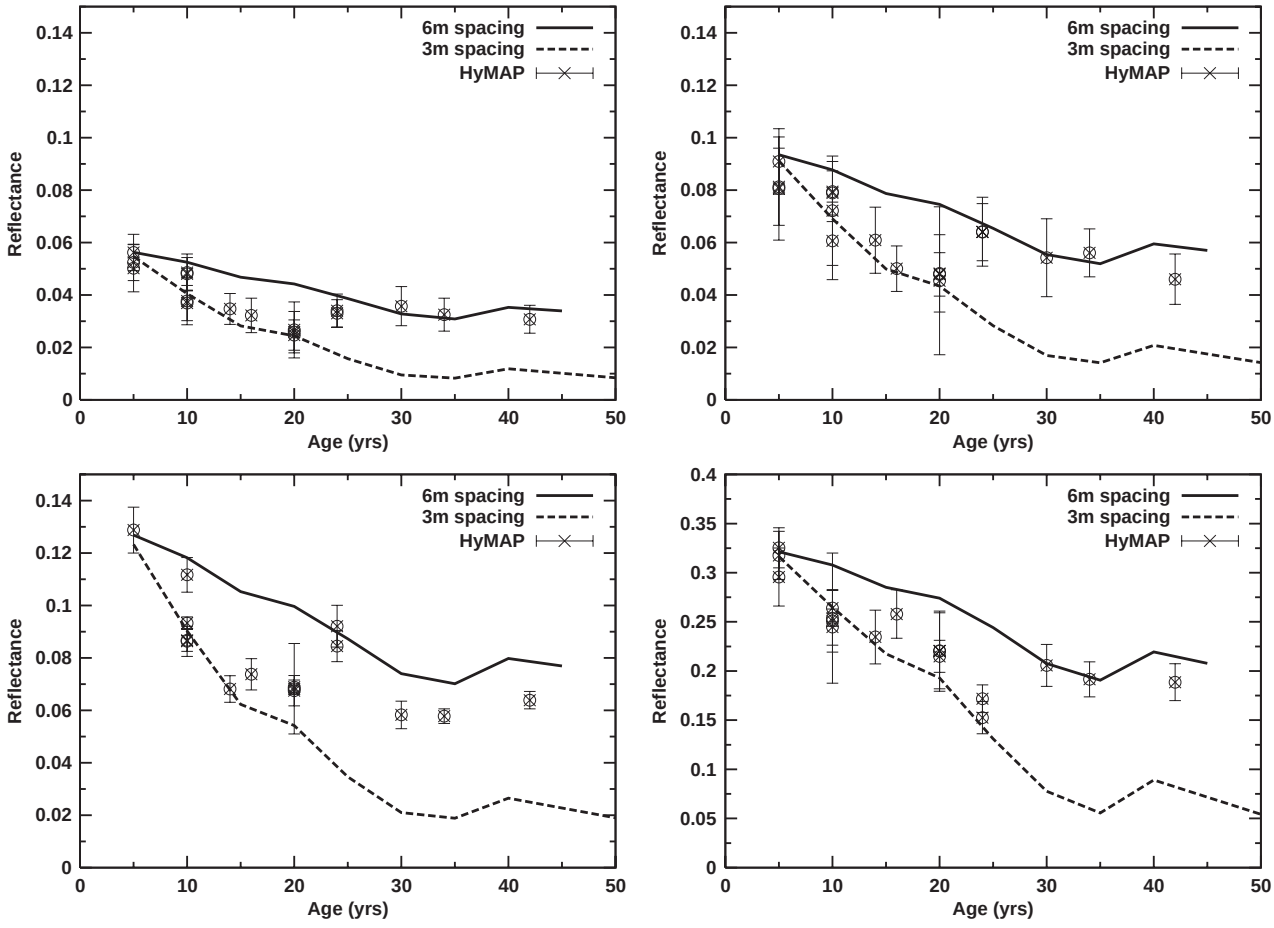

Fig. 10. Comparison of simulated and observed forest canopy reflectance in the optical: 446 nm (upper left), 546 nm (upper, right), 646 nm (lower left) and 844 nm (lower right). The upper and lower lines in each case represent reflectance for the low (6 m spacing) and higher density (3 m spacing) canopies, respectively.

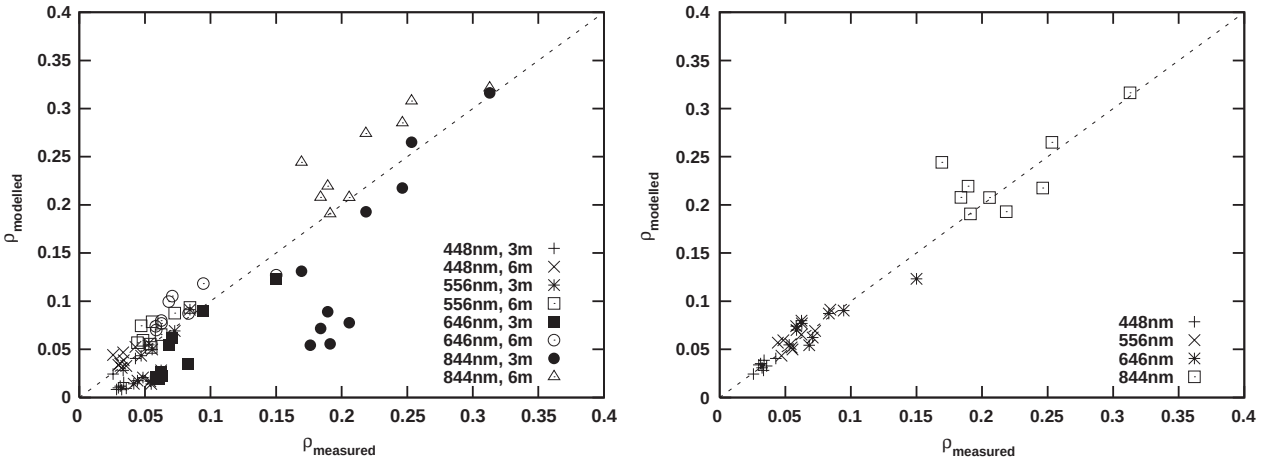

Fig. 11. Scatter of $\rho_{measured}$ against $\rho_{modelled}$. a) Shows results of regression assuming no preference for a specific tree density at a given age; b) Modelled values are regressed against the 3 m spacing canopy results for age $\leq$20 years, and against 6 m spacing thereafter.

a measured against modelled backscatter values for all bands and polarisations in L-band and X-band VV polarisation.

4. Discussion

4.1. Optical

In each case in Fig. 10, modelled results are presented from two canopy structure scenarios: the solid line represents average tree spacing of 6 m, while the dashed line represents average tree spacing of 3 m. As described above, tree spacing in Thetford Forest is initially around 2 m but rises to between 4 and 6 m from around 20 years onwards following thinning. The comparison shown in Figs. 10 and 11 demonstrates that the optical domain simulations of canopy reflectance are generally in good agreement with the HyMAP observations, particularly given the variability of observed reflectance for given age. This variability is illustrated by the range of observed values of NIR reflectance at age 10, where reflectance varies from less than 0.2 to greater than 0.33. What is clear from Fig. 10 is that the radiometric simulations driven by the structural model encompass the observations rather well i.e. the 3D model representations of canopy structure coupled with the optical simulations are able to encompass the observed range of reflectance variation. It is also clear from Fig. 10 that there is not a great deal of variation in observed reflectance with age in the HyMAP data. However, interestingly there is a noticeable increase in observed reflectance between 20 and 30 years of age, particularly at the NIR wavelength. The observed reflectance values move from the lower range of modelled values, corresponding to the dense 3 m canopy spacing, towards the upper range, corresponding to the less dense 6 m canopy spacing. From Fig. 11a it is clear that there is better agreement between modelled and measured reflectance values for the dense canopy at younger ages, and similarly for the less dense canopy at older ages. This is highlighted in Fig. 11b where the same results are shown, but with only the 3 m spacing canopy model results included up to and including 20 years, and only 6 m spacing model results used after this. Clearly the regression results are much better in the latter case, with r^2 values rising from 0.89 to 0.98.

This suggests that the simulated reflectances are actually capturing the changes in reflectance due to the thinning of the forest that occurs between 20 and 25 years rather well. The agreement in Fig. 11b between modelled and measured results is good and indicates that a LUT-based inversion approach would be ideal in this case. Pre-computed values of reflectance in a LUT would encompass a range of realisations of canopy structure and hence reflectance. The match with observations could then be made with the corresponding appropriate canopy structure. The agreement shown in Fig. 11b indicates that this would be effective despite the fact that there is relatively small sensitivity to age variation within the HyMAP observations. One issue not considered here is that over- or under-estimate of the value of the atmospheric optical depth, τ, used in the atmospheric correction procedure will have a disproportionate effect in the visible part of the spectrum, due to increased atmospheric scattering at shorter wavelengths (Kaufmann, 1989). However, a LUT-based approach can even include τ as a retrieval parameter, via multiple simulations of the atmospheric contribution to measured reflectance (Lewis et al., 2003).

4.2. Microwave

In the microwave domain, Fig. 12 shows that the L- and X-band model predictions are essentially unaffected by tree spacing for all but the largest spacings (20 m) in which case the backscattered power is significantly lower. In all simulations (at both L- and X-bands) the dominant contribution to the scattering is directly from the trees themselves, and scattering from the ground or ground-vegetation double bounce is much lower. The comparison between modelled and observed backscattered values in Fig. 13 shows that agreement is reasonable in many cases. The insensitivity of the measured signal to canopy age seen in the optical data is somewhat different for the microwave observations, with a

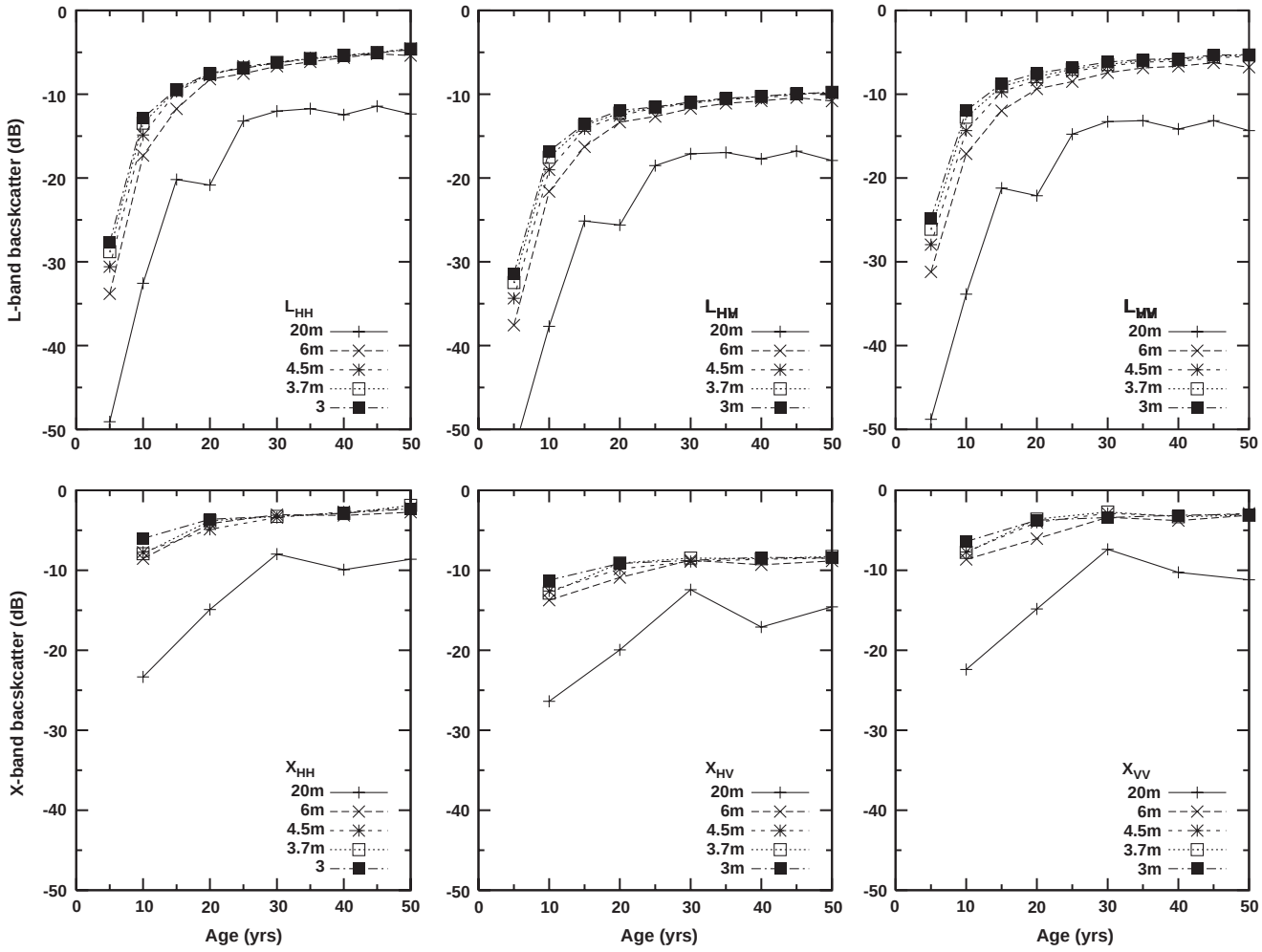

Fig. 12. Modelled microwave backscatter values with age for L-band (top row, left-to-right are HH, HV and VV polarisations), and X-band (bottom row, left-to-right are HH, HV and VV polarisations).

high sensitivity for younger canopies but with all simulations showing a saturation in the scattered power at around 25–30 years.

The model predictions in Fig. 13 underestimate the observed data at low ages (very noticeably) and tend to overestimate the observed data for older trees (by up to 2 dB). This discrepancy between younger and older canopies is similar to that seen in the optical comparisons in Fig. 10, although the sensitivity of modelled backscatter to tree spacing is much lower than the sensitivity of modelled reflectance.

For the comparisons of X-band modelled and measured backscatter shown in Fig. 14, the more extreme variation of spacing clearly brackets the observations at the early stages but narrowly fails to do so at later stages. In the younger cases shown in Figs. 13 and 14 (<25 years) it should be noted that both the L- and X-band simulations are dominated by the ground at low ages and the underprediction of modelled backscatter is likely to be either a consequence of an incorrect representation of the ground scattering or the fact that understory vegetation is not included in the model. Fig. 14b shows the scatter of measured against modelled results is greater in the microwave simulations. However, given that the variability of observed backscatter is up to 10 dB at any given age this is perhaps not surprising. This is reflected in r^2 values of between 0.22 and 0.6.

5. Conclusions

Results presented above show that, given a suitable 3D structural model of the development of forest canopy architecture, it is possible to drive both optical and microwave scattering models using the same structural description. The reason for such an approach is to establish that, if such architectural models can be interfaced successfully with both optical and microwave scattering models, then they can be used to: i) simulate and understand the canopy scattering signal in both the optical and microwave domains (in particular, the impact of canopy structure in this signal); and ii) establish a framework for combining optical and microwave data for biophysical parameter retrieval problems. Such an approach has the potential for greatly improving biophysical parameter retrieval from EO data by combining the advantages of both wavelength regimes.

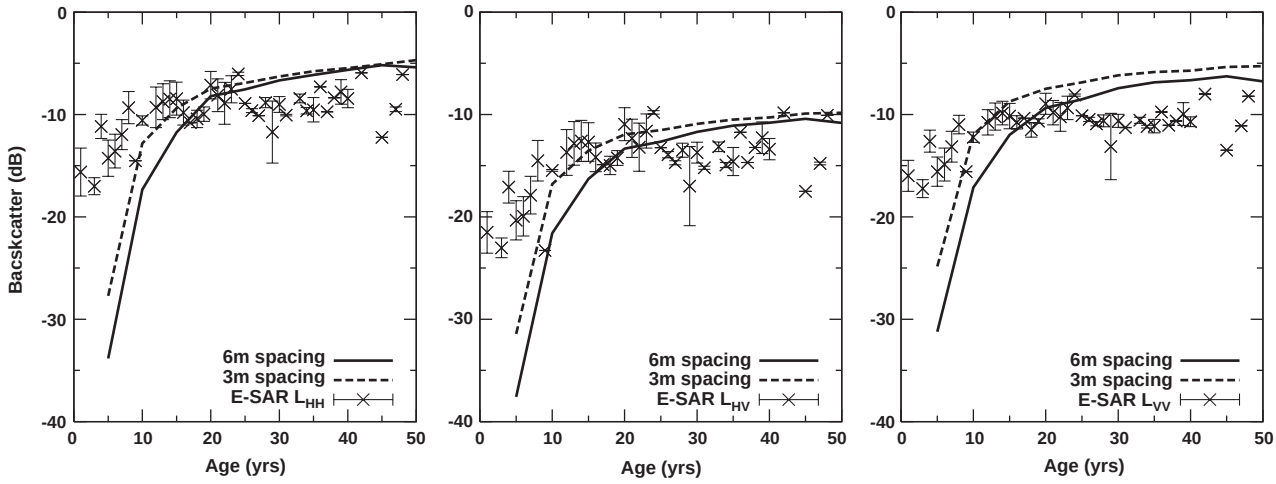

Fig. 13. Comparison of modelled and measured microwave backscatter values with age for L-band (left-to-right are HH, HV and VV polarisations), with varying canopy density.

For large, complex canopies such as those described here (containing $\approx 10^{10}$ scattering primitives) it has only been recently possible to contemplate simulating the scattering behaviour in the optical domain, such as by Monte Carlo methods, because of the number of calculations involved. Even with advances in computing power highly efficient scattering models are required. As a result, typical numerical inversion methods are not useful for trying to retrieve biophysical parameters using such detailed 3D models. However the models can be used to generate LUTs of canopy radiometric response for a range of canopy scenarios, at arbitrary wavelengths (including thermal, although that is not covered here). This potentially allows the retrieval of canopy parameters from combined optical and microwave EO datasets (Saich et al., 2003).

In this study, an architectural model of Scots pine was used to generate individual trees for various stages of growth from 5 to 50 years of age. The driving parameter of the architectural model, the light extinction regime within the canopy, was optimised iteratively to generate trees with height and dbh parameters corresponding to values observed within a managed Scots pine forest at Thetford, in the UK. Individual modelled trees were replicated to generate 3D structural models of entire forest canopy scenes covering the available range of observed tree spacing (according to management records for Thetford Forest). The resulting architectural models, along with a description of the wavelength-dependent scattering properties of the media comprising the canopy (needles, bark, soil, understory vegetation) were used to simulate the radiation regime of the Scots pine canopy at various stages of growth. The size, shape and distribution (phyllotaxy) of needles at the shoot level were compared with representations used in other studies. These parameters, particularly needle shape and phyllotaxy, were shown to be of importance in the optical simulations of reflectance, particularly in the NIR where multiple scattering is significant. The impact of needle shape and phyllotaxy tends to be smoothed out in moving from shoot to canopy scale but needle shape in particular can influence the total absorbed radiation within the canopy and hence the reflected signal available to be measured remotely.

It was shown that the simulated optical and microwave canopy response agreed quite well in some cases with optical and microwave observations collected over Thetford Forest. The

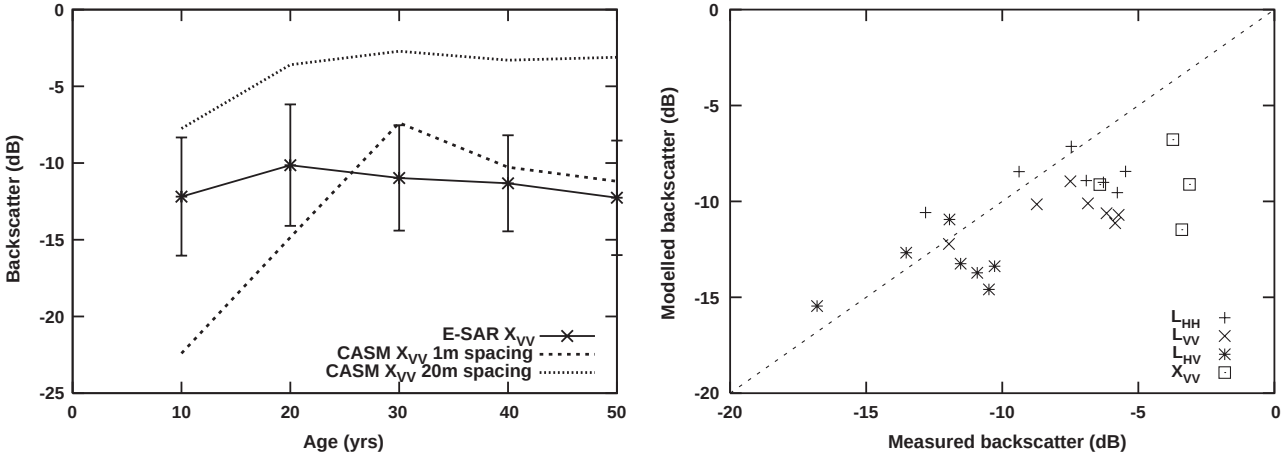

Fig. 14. Comparison of modelled and measured microwave backscatter values with age for X-band with varying canopy density. a) Shows comparison with two extreme model realisations (1 and 20 m tree spacing); b) shows modelled against measured results for all microwave cases.

optical simulations were shown to bracket the observations in all cases. The discontinuity in observed reflectance with age as a result of thinning was captured by the model simulations in moving from high to low density canopy realisations. This is despite the relative insensitivity of the observed reflectance with canopy age. This insensitivity is likely to be in part due to the presence of canopy understory dominated by relatively homogeneous green vegetation. This means that even when solar radiation penetrates the canopy, it tends to be scattered/absorbed by green vegetation with a similar spectral response to the tree canopy itself. The understory is also more likely to influence the signal at younger ages and/or stands of lower density and will therefore reduce sensitivity of the measured signal with age. In future studies, the use of more realistic description of the understory (such as a detailed 3D model) may improve sensitivity of the modelled signal for lower density/age stands. As a result of these factors, in order to differentiate stands of different ages a signal more sensitive to variations in structure is required, such as more suitable angular configuration. Unfortunately, the HyMAP data available for this study were flown more than 40° away from the solar principal plane where the angular signature is known to be strongest (Liang, 2004). What small variation there is arises from variability within the stands rather than as a result of varying view zenith angle. This is confirmed by analysis demonstrating only small variation of reflectance with view zenith angle (Saich et al., 2003). This lack of angular signal is also partly due to the fact that many of the forest stands are located towards the centre of an already narrow instrument swath and the potential for view zenith angle variation is not all that high, regardless of whether sampling were in the solar principal plane or not.

Despite the various issues with the EO data used, the feasibility of using full 3D descriptions of canopy structure (including location of all needles) to simulate arbitrarily complex forest canopy scenarios was demonstrated. Using efficient 3D scattering models allows the reflectance and backscatter of complex scenes to be carried out in typically 10–100 s of minutes per view angle per scene (Lewis, 1999; Pinty et al., 2004). Even in extreme cases (very dense canopies), we have shown that it is possible to use full descriptions of 3D canopy architecture, down to the level of individual needles, to simulate reflectance and backscatter of canopy stands. In this way LUTs of canopy response in both optical and microwave domains can be generated in a few days using a common canopy structure, which in turn can be used to generate biophysical parameters from remote sensing observations (i.e. to solve the inverse problem). The application of such an approach to the inverse problem and, in particular, the implications for understanding the impact of uncertainty in retrieved parameter, is the subject of ongoing work and will be discussed elsewhere.

Acknowledgements

This work was funded under ESA contract AO/1-3679/00/NL/NB: Development of Architectural Vegetation Growth Models for Remote Sensing Applications. Funding for some of this work was also provided by the NERC Centre for Terrestrial Carbon Dynamics. Thanks to Heiko Balzter (CEH Monks Wood), Dr. Adrian Luckman and Dr. Laine Skinner (University of Wales, Swansea) for access to field measurements and SAR data, to Dr. Sebastien Lafont for provision of forestry data from Thetford Forest, to Dr. Risto Sievänen for information on Finnish Scots pine growth and to B. Hosgood at the EGO facility, JRC Ispra, for making the LOPEX93 data available. We are grateful also to the positive and helpful comments of the anonymous referees of this manuscript.

Appendix A

The following tables give the default parameter values used in the Treegrow model for generation of Scots pine canopies in this simulation study. All other variables (and modifications thereof) are described above.

Table A1
Treegrow species characteristics

Number of shoot types	2
Maximum number of flushes per year	1
Number of shoot orders	4
Minimum shoot length (cm)	1
Maximum age of shoots with leaves (yr)	6
Maximum stagnation time of a shoot (yr)	6
Maximum tolerable light reduction (%)	75
Plagiotropy order >1	Yes
Shoot type conversion	Yes
Sympodial growth	No
Terminal flowering	No

Table A2
Treegrow shoot length parameters

	Shoot type 1	Shoot type 2
L1 (0–1)	0.6	0.350
L2	1	1
L3 (>0)	5.0	5.0
L4 (>0)	0.4	0.4
L5 (0–1)	0.2	0.2

Table A3
Treegrow shoot number parameters (child shoots per parent shoot)

	Shoot type 1	Shoot type 2
N0 (1–31)	1	0
N1	1.43	0.42
N2	0.41	0.94
F1 (%)	0.4	0.4
F2 (>0)	0.5	0.5
Probability of reiteration	1	1
Maximum age of potential reiteration	6	6

Table A4
Treegrow shoot distribution parameters

	Shoot type 1	Shoot type 2
Random distribution	Yes	Yes
Max. dist. from shoot base to top of parent/parent length (0–1)	0.6	0.9
Opposite buds distribution	No	No

Table A5
Treegrow shoot diameter parameters

	Shoot type 1	Shoot type 2
D1 (>0)	0.12	0.12
D2 (>0)	0.650	0.650
D3 (>0)	0.670	0.670

Table A6
Treegrow angle-of-side-shoot-with-parent-shoot parameters

	Shoot type 1	Shoot type 2
A1 (0–180)	45.0	60.0
A2 (0–180)	30.0	30.0
A3 (0–180)	60.0	90.0

Table A7
Treegrow angle-of-continuing-shoot-with-parent-shoot parameters

	Shoot type 1	Shoot type 2
A4 (−100–100)	−2.0	−2.0
A5 (0–10)	0	0
A6 (0–180)	15.0	15.0
A7 (0–180)	2.0	2.0

Table A8
Treegrow shoot inclination increment parameters

I1	0.17
I2	0.22
I3	0.05

Table A9
Treegrow shoot mortality parameters

M1	0.17
M2	0.22
M3	0.05
Max. branch length/diameter ratio	160.0
B1 (>0)	10.0
B2 (>0)	1.2
Max. diameter (mm) of living shoots that may break off by accident	5.0
Accidental breakoff probability (%)	0.01

References

Balzter, H., Saich, P., Luckman, A., Skinner, J., & Grant, L. (2001). Forest stand structure from airborne polarimetric InSAR. *Proceedings of 3rd international symposium on retrieval of bio- and geophysical parameters from SAR data for land applications, Sheffield, UK, 11–14th September 2001, ESA SP-475* (pp. 321–326).

Boardman, J. (1998). Post-ATREM polishing of AVIRIS apparent reflectance data using EFFORT: A lesson in accuracy versus precision. *Summaries of Seventh JPL Airborne Earth Science Workshop*, *vol. 1* (p. 53).

Cannell, M. G. R., & Bowler, K. C. (1978). Phyllotactic arrangements of needles on elongating conifer shoots: A computer simulation. *Canadian Journal of Forest Research*, *8*, 138–141.

Cermák, J., Riguzzi, F., & Ceulemans, R. (1998). Scaling up from the individual tree to the stand level in Scots pine: I. Needle distribution, overall crown and root geometry. *Annales des Sciences Forestieres*, *55*(1–2), 63–88.

Cescattti, A. (1998). Effects of needle clumping in shoots and crowns on the radiative regime of a Norway spruce canopy. *Annales des Sciences Forestieres*, *55*(1–2), 89–102.

Cocks, T., Jensen, R., Stewart, A., Wilson, I. and Shields, T. (1998). The HyMAP Airborne hyperspectral sensor: The system, calibration and performance. Presented at 1st EARSEL workshop on imaging spectroscopy, Zurich, October 1998.

Courbaud, B., de Coligny, F., & Cordonnier, T. (2003). Simulating radiation distribution in a heterogeneous Norway spruce forest on a slope. *Agriculture and Forest Meteorology*, *116*(1), 1–18.

Dawson, T. P., Curran, P. J., & Plummer, S. E. (1998). LIBERTY — Modelling the effects of leaf biochemical concentration on reflectance spectra. *Remote Sensing of Environment*, *65*, 50–60.

Disney, M. I., Lewis, P., Nichol, C., & Quaife, T. (2005). Exploring the relationship between vegetation canopy structural and radiometric behaviour. *In proc. ISMPSRS05, Beijing, 17–19 October 2005*.

Disney, M. I., Lewis, P., & North, P. R. J. (2000). Monte Carlo ray tracing in optical canopy reflectance modelling. *Remote Sensing Reviews*, *18*(2–4), 163–196.

Disney, M. I., Lewis, P., & Saich, P. (2004). 3D structural modelling of conifer canopies for remote sensing simulations and parameter estimation. In C., Godin, et al., (Ed.), *Proc. 4th international workshop on functional–structural plant models, 7–11 June 2004, Montpellier, France* (p. 282).

Godin, C., & Sinoquet, H. (2005). Functional–structural plant modelling. *New Phytologist*, *166*, 705–708.

Goel, N. S. (1988). Models of vegetation canopy reflectance and their use in the estimation of biophysical parameters from reflectance data. *Remote Sensing Reviews*, *4*, 1–222.

Goel, N. S. (1992, 1989). Inversion of canopy reflectance models for estimation of biophysical parameters from reflectance data. In G. Asrar (Ed.), *Remote sensing reviews, theory and applications of optical remote sensing* (pp. 205–251). New York: J. Wiley and Sons.

Goel, N. S., & Strebel, D. E. (1983). Inversion of vegetation canopy reflectance models for estimating agronomic variables: 1. Problem definition and initial results using the Suits model. *Remote Sensing of Environment*, *13*, 487–507.

Goel, N. S., & Thompson, R. L. (2000). A snapshot of canopy reflectance models, and a universal model for the radiation regime. *Remote Sensing Reviews*, *18*, 197–225.

Hallikainen, M. T., Ulaby, F. T., Dobson, M. C., El-Rayes, M. A., & Wu, L. (1985). Microwave dielectric behaviour of wet soil: Part I. Empirical models and experimental observations. *IEEE Transactions on Geoscience and Remote Sensing*, *23*, 25–34.

Hosgood, B., Jaquemoud, S., Andreoli, G., Verdebout, J., Pedrini, G., & Schmuck, G. (1995). Leaf optical properties experiment 93 (LOPEX93). Ispra Italy: European Commission, Joint Research Centre Institute of Remote Sensing Applications.

Imhoff, M. L. (1995). A theoretical analysis of the effect of forest structure on synthetic aperture radar backscatter and the remote sensing of biomass. *IEEE Transactions on Geoscience and Remote Sensing*, *33*(2), 341–352.

Jacquemoud, S., & Baret, F. (1990). PROSPECT — A model of leaf optical properties spectra. *Remote Sensing of Environment*, *34*(2), 75–91.

Jacquemoud, S., Ustin, S. L., Verdebout, J., Schmuck, G., Andreoli, G., & Hosgood, B. (1996). Estimating leaf biochemistry using the PROSPECT leaf optical properties model. *Remote Sensing of Environment*, *56*(3), 194–202.

Karam, M. A., & Fung, A. K. (1988). Electromagnetic scattering from a layer of finite randomly oriented, dielectric circular cylinder over a rough interface with application to vegetation. *International Journal of Remote Sensing*, *9*, 1109–1134.

Karam, M. A., Fung, A. K., & Antar, Y. M. M. (1988). Electromagnetic wave scattering from some vegetation samples. *IEEE Transactions on Geoscience and Remote Sensing*, *26*, 799–808.

Kaufmann, Y. J. (1989). The atmospheric effect on remote sensing and its correction. In G. Asrar (Ed.), *Theory and applications of optical remote sensing* (pp. 336–428). New York: Wiley and Sons.

Kimes, D. S., Knyazikhin, Y., Privette, J. L., Abuelgasim, A. A., & Gao, F. (2000). Inversion methods for physically-based models. *Remote Sensing Reviews*, *18*, 381–439.

Kimes, D. S., Nelson, R. F., Manry, M. T., & Fung, A. K. (1998). Attributes of neural networks for extracting continuous vegetation variables from optical

and radar measurements. *International Journal of Remote Sensing*, *19*, 2639–2663.

Kimes, D. S., Ranson, K. J., & Sun, G. (1997). Inversion of a forest backscatter model using neural networks. *International Journal of Remote Sensing*, *18*, 2181–2199.

Knyazikhin, Y., Kranigk, J. V., Myneni, R. B., Panferov, O., & Gravenhorst, G. (1998a). Influence of small-scale structure on radiative transfer and photosynthesis in vegetation cover. *Journal of Geophysical Research*, *103*, 6133–6144.

Knyazikhin, Y., Marshak, A., & Myneni, R. B. (2005). Three-dimensional radiative transfer in vegetation canopies. In A. Davis, & A. Marshak (Eds.), *Three-dimensional radiative transfer in the cloudy atmosphere*. New York: Springer-Verlag, ISBN: 3-540-23958-8.

Knyazikhin, Y., Martonchik, J. V., Myneni, R. B., Diner, D. J., & Running, S. W. (1998b). Synergistic algorithm for estimating vegetation canopy leaf area index and fraction of absorbed photosynthetically active radiation from MODIS and MISR data. *Journal of Geophysical Research*, *103*(D24), 32257–32276.

Kurth, W., & Sloboda, B. (1997). Growth grammars simulating trees — An extension of L-systems incorporating local variables and sensitivity. *Silva Fennica*, *31*, 285–295.

Lang, R. H., Chauhan, N. S., Ranson, K. J., & Kilic, O. (1994). Modelling P-band SAR returns from a Red pine stand. *Remote Sensing of Environment*, *47*, 132–141.

Leersnijder R.P. (1992). *PINOGRAM: A pine growth area model.* WAU dissertation 1499, Wageningen Agricultural University, The Netherlands.

Lewis, P. (1999). Three-dimensional plant modelling for remote sensing simulation studies using the Botanical Plant Modelling System (BPMS). *Agronomie, Agriculture and Environment*, *19*(3–4), 185–210.

Lewis, P., Barnsley, M., Quaife, T., Thackrah, G., Disney, M. I., & Saich, P. (2003). Biophysical parameters from CHRIS/PROBA. *Proc. SPECTRA workshop, ESA/ESTEC Noordwijk, Netherlands, Oct. 28–30*.

Lewis, P., Saich, P., Disney, M. I., Andrieu, B., Fournier, C., Macklin, T., et al. (2004). Calibration of an L-system model of winter wheat for remote sensing modelling and inversion. In Godin C., et al., (Eds.), *Proc. 4th international workshop on functional–structural plant models, 7–11 June 2004, Montpellier, France* (pp. 257–261).

Li, X., & Strahler, A. H. (1985). Geometrical–optical modelling of a conifer forest canopy. *IEEE Transactions on Geoscience and Remote Sensing*, *23*, 705–721.

Li, X., & Strahler, A. H. (1986). Geometrical–optical reflectance modelling of a conifer forest canopy. *IEEE Transactions on Geoscience and Remote Sensing*, *24*, 906–919.

Liang, S. (2004). *Quantitative remote sensing of land surfaces*. New Jersey: Wiley and Sons.

Lin, Y. C., & Sarabandi, K. (1999). A Monte Carlo coherent scattering model for forest canopies using fractal generated trees. *IEEE Transactions on Geoscience and Remote Sensing*, *37*, 440–451.

Lin, Y. C., & Sarabandi, K. (1999). Retrieval of forest parameters using a fractal-based coherent scattering model and a genetic algorithm. *IEEE Transactions on Geoscience and Remote Sensing*, *37*, 1415–1424.

Mäkelä, A., Landsberg, J., Ek, A. R., Burk, T. E., Ter-Mikaelian, M., Ågren, G. I., et al. (2000). Process-based models for forest ecosystem management: Current state of the art and challenges for practical implementation. *Tree Physiology*, *20*, 289–298.

Mêch, R., & Prusinkiewicz, P. (1996). Visual models of plants interacting with their environment. *Proceedings of SIGGRAPH 96 (New Orleans, Louisiana, August 4–9, 1996). In computer graphics proceedings, annual conference series, ACM SIGGRAPH* (pp. 397–410).

Moghaddam, M., & Saatchi, S. (1995). Analysis of scattering mechanisms in SAR imagery over boreal forest: Results from BOREAS '93. *IEEE Transactions on Geoscience and Remote Sensing*, *33*(5), 1290–1296.

Moghaddam, M., & Saatchi, S. (1999). Monitoring tree moisture using an estimation algorithm applied to SAR data from BOREAS. *IEEE Transactions on Geoscience and Remote Sensing*, *37*, 901–916.

Myneni, R. B., Ross, J., & Asrar, G. (1989). A review on the theory of photon transport in leaf canopies. *Agriculture and Forest Meteorology*, *45*, 1–153.

Oker-Blom, P., & Smolander, H. (1988). The ratio of shoot silhouette area to total needle area in Scots pine. *Forest Science*, *34*, 894–896.

Panferov, O., Knyazikhin, Y., Myneni, R. B., Szarzynski, J., Engwald, S., Schnitzler, K. G., et al. (2001). The role of canopy structure in the spectral variation of transmission and absorption of solar radiation in vegetation canopies. *IEEE Transactions on Geoscience and Remote Sensing*, *39*(2), 241–253.

Perttunen, J., Sievanen, R., Nikinmaa, E., Saluminen, H., Saarenmaa, H., & Vakeva, J. (1996). LIGNUM: A tree model based on simple structural units. *Annals of Botany*, *77*, 87–98.

Pierce, L. E., Sarabandi, K., & Ulaby, F. T. (1995). Application of an artificial neural network in canopy scattering inversion. *International Journal of Remote Sensing*, *15*, 3263–3270.

Pinty, B., Gobron, N., Widlowski, J. -L., Gerstl, S. A. W., Verstraete, M. M., Antunes, M., et al. (2004). RAMI II: The second radiative transfer model intercomparison exercise. *Journal of Geophysical Research*, *109*(D6), D06210.

Pinty, B., & Verstraete, M. M. (1991). Extracting information on surface properties from bidirectional reflectance measurements. *Journal of Geophysical Research*, *96*, 2865–2874.

Price, J. C. (1990). On the information-content of soil reflectance spectra. *Remote Sensing of the Environment*, *33*(2), 113–121.

Proisy, C., Mougin, E., Fromard, F., Trichon, V., & Karam, M. A. (2002). On the influence of canopy structure on the radar backscattering of mangrove forests. *International Journal of Remote Sensing*, *23*(20), 4197–4210.

Qin, W., & Liang, S. (2000). Plane-parallel canopy radiative transfer modelling: Recent advances and future directions. *Remote Sensing Reviews*, *18*, 281–305.

Ranson, K. J., Sun, G., Weishampel, J. F., & Knox, R. G. (1997). Forest biomass from combined ecosystem and radar backscatter modeling. *Remote Sensing of Environment*, *59*, 118–133.

Rautiainen, M., & Stenberg, P. (2005). Application of photon recollision probability in coniferous canopy reflectance simulations. *Remote Sensing of Environment*, *96*, 98–107.

Reffye, Ph. de, Fourcaud, T., Blaise, F., Barthelemy, D., & Houllier, F. (1997). A functional model of tree growth and architecture. *Silva Fennica*, *31*, 297–311.

Reffye, Ph. de, Houllier, F., & Blaise, F. (1999). Modelling plant growth and architecture. In F. Blasco, & A. Weill (Eds.), *Advances in environment and ecological modelling* (pp. 70–72). New York: Elsevier.

Ross, J. K. (1981). *The radiation regime and architecture of plant stands*. Netherlands: W. Junk, The Hague.

Saatchi, S., & Moghaddam, M. (2000). Estimation of crown and stem water content and biomass of boreal forest using polarimetric SAR imagery. *IEEE Transactions on Geoscience and Remote Sensing*, *38*, 697–709.

Saich, P., Lewis, P., Disney, M. I., & Thackrah, G. (2001). Comparison of HyMAP/E-SAR data with models of optical reflectance and microwave scattering from vegetation canopies. *Proceedings of 3rd international symposium on retrieval of bio- and geophysical parameters from SAR data for land applications, Sheffield, UK, 11–14th September 2001, ESA SP-475* (pp. 75–80).

Saich, P., Lewis, P., Disney, M., van Oevelen, I., Woodhouse, P., Andrieu, I., et al. (2003). Development of vegetation growth models for remote sensing applications. Final report of ESA contract AO/1-3679/00/NL/NB (available from http://www.geog.ucl.ac.uk/~psaich/esa).

Sievänen, R., Nikinmaa, E., Nygren, P., Ozier-lafontaine, H., Perttunen, J., & Hakula, H. (2000). Components of functional–structural tree models. *Annals of Forest Science*, *57*(5/6), 399–412.

Smolander, S., & Stenberg, P. (2003). A method to account for shoot scale clumping in coniferous canopy reflectance models. *Remote Sensing of the Environment*, *88*, 363–373.

Smolander, S., & Stenberg, P. (2005). Simple parameterizations of the radiation budget of uniform broadleaved and coniferous canopies. *Remote Sensing of Environment*, *94*, 355–363.

Stenberg, P., Palmroth, S., Bond, B. J., Sprugel, D. G., & Smolander, H. (2001). Shoot structure and photosynthetic efficiency along the light gradient in a Scots pine canopy. *Tree Physiology*, *21*, 805–814.

Strahler, A. H. (1996). Vegetation canopy reflectance modeling: Recent developments and remote sensing perspectives. *Remote Sensing Reviews*, *15*, 179–194.

Sun, G. Q., & Ranson, K. J. (1995). A 3-dimensional RADAR backscatter model of forest canopies. *IEEE Transactions on Geoscience and Remote Sensing*, *33*, 372–382.

Sun, G. Q., Simonett, D. S., & Strahler, A. H. (1991). A RADAR backscatter model for discontinuous forest canopies. *IEEE Transactions on Geoscience and Remote Sensing*, *29*(4), 639–650.

Tsang, L., Kong, J. A., & Shin, R. T. (1985). *Theory of microwave remote sensing*. New York: J. Wiley and Sons.

Ulaby, F. T., Moore, R. K., & Fung, A. K. (1986). *Microwave remote sensing: Radar remote sensing and surface scattering and emission theory (remote sensing library)*. Norwood, MA, USA: Artech House.

Wang, Y., Buermann, W., Stenberg, P., Smolander, H., Hame, T., Tian, Y., et al. (2003). A new parameterization of canopy spectral response to incident solar radiation: Case study with hyperspectral data from pine dominant forest. *Remote Sensing of Environment*, *85*, 304–315.

Weiss, M., Baret, F., Myneni, R. B., Pragnere, A., & Knyazikhin, Y. (2000). Investigation of a model inversion technique to estimate canopy biophysical variables from spectral and directional reflectance data. *Agronomie*, *20*(1), 3–22.

Widlowski, J. -L., Pinty, B., Gobron, N., Verstraete, M. M., Diner, D. J., & Davis, A. B. (2004). Canopy structure parameters derived from multi-angular remote sensing data for terrestrial carbon studies. *Climatic Change*, *67*, 403–415.

Woodhouse, I. H., & Hoekman, D. H. (2000). Radar modelling of coniferous forest using a tree growth model. *International Journal of Remote Sensing*, *21*, 1725–1737.